Local structures around 3*d* metal dopants in topological insulator Bi_2Se_3 studied by EXAFS measurements

Zhen Liu,[1] Xinyuan Wei,[1] Jiajia Wang,[1] Hong Pan,[1] Fuhao Ji,[1] Fuchun Xi,[1] Jing Zhang,[2] Tiandou Hu,[2] Shuo Zhang,[3] Zheng Jiang,[3] Wen Wen,[3] Yuying Huang,[3] Mao Ye,[4] Zhongqin Yang,[1,*] and Shan Qiao[4,5,†]

[1]*Department of Physics, State Key Laboratory of Surface Physics, and Laboratory of Advanced Materials, Fudan University, Shanghai 200433, People's Republic of China*

[2]*Synchrotron Radiation Facility, Institute of High Energy Physics, Chinese Academy of Sciences, Beijing 100039, People's Republic of China*

[3]*Shanghai Synchrotron Radiation Facility, Shanghai Institute of Applied Physics, Chinese Academy of Sciences, Shanghai 201800, People's Republic of China*

[4]*State Key Laboratory of Functional Materials for Information, Shanghai Institute of Microsystem and Information Technology, Shanghai, 200050, People's Republic of China*

[5]*School of Physical Science and Technology, ShanghaiTech University, Shanghai, People's Republic of China*

(Received 5 April 2014; revised manuscript received 25 August 2014; published 8 September 2014)

Transition-metal-doped Bi_2Se_3 crystals, $X_{0.05}Bi_2Se_3$ (X = Cr, Co, Ni, and Cu), are prepared and studied by powder x-ray diffraction and extended x-ray absorption fine structure (EXAFS) measurements to get the local structures around the dopants. Cr atoms substitute Bi atoms and Co atoms may substitute Bi atoms or form Co_3Se_4 ($C2/m$) clusters. Cu is also found taking the Bi substitutional site, which differs from the reported superconductor phase of Cu-doped Bi_2Se_3, suggesting the dependence of site occupancy of Cu in Bi_2Se_3 on the process of sample growing. For $Ni_{0.05}Bi_2Se_3$, Ni atoms form Ni_3Se_4 ($C2/m$) clusters. The nearest neighbors of X (X = Cr, Co, and Cu) are Se atoms, and the X-Se bond lengths are extracted from EXAFS as 2.50 Å for Cr-Se, 2.40 Å for Co-Se, and 2.38 Å for Cu-Se, which show the direct evidences of dramatic structural relaxations around 3*d* dopants. The bond information of local structures around dopants is valuable for subsequent theoretical studies, and can hardly be obtained from other techniques.

DOI: 10.1103/PhysRevB.90.094107 PACS number(s): 61.05.cp, 61.05.cj

I. INTRODUCTION

Topological insulators (TIs) have dissipationless surface states, which have Dirac-type energy dispersion and helical spin polarization. The surface states are protected by the topological properties of the bulk bands and are supposed to be robust to disorder, interaction, and thermal fluctuations, potentially leading to dissipationless device applications [1–6].

Recently, 3*d*-metal-doped TIs have attracted much attention because some exotic quantum phenomena may be achieved in these systems. A topological supercondutor phase in Cu-doped Bi_2Se_3 provides an opportunity to realize Majorana fermions [7,8]. Ferromagnetic TIs are supposed to induce several topological quantum phenomena, such as quantized anomalous Hall effect (QAHE) [9], topological quantized magnetoelectric effect [10], and the magnetic monopole [11]. Electronic junctions between TIs and ferromagnetic-doped TIs are feasible for their intrinsic chemical and structural compatibility and such junctions are promising for studying novel physics and new types of electronic devices. Experimentally, ferromagnetism has been realized in several magnetically doped TIs [12–19], and even QAHE has been discovered in a CrBiSbTe system which realizes a dissipationless current without magnetic field [20]. To study the mechanism of the magnetisms in TIs, the information about the locations and the local structures around the dopants is important because the occupied sites of the dopants can extremely affect the properties of the entire crystal. For example, Cu-doped Bi_2Se_3 can be superconducting when Cu is in the van der Waals (vdW) gap, while it is normal when Cu occupies other sites [8,21,22]

Several theoretical researches on transition-metal-doped TIs suppose that the 3*d* dopants tend to occupy the Bi substitutional sites [9,23], which is doubtable considering the big differences between atomic radii of Bi and 3*d* metal atoms. Transmission electron microscope (TEM) and scanning tunneling microscope (STM) measurements of copper-doped Bi_2Se_3 show that Cu atoms prefer intercalation or interstitial sites to Bi substitutional sites [8,21,22]. For Mn dopants, Mn atoms are found to substitute on the Bi sites randomly in Bi_2Te_3 crystals [12], but form Mn clusters in Bi_2Se_3 crystals [19]. These findings all indicate that the location of 3*d* impurities in TIs may be more complex than expected. Although theoretical studies on site preferences of 3*d* impurities in Bi_2Se_3 crystals have been reported [24–26], the direct experimental measurements of local atomic structures around the dopants are significant to understand the mechanism of magnetism and possible topological behaviors in the compounds. X-ray absorption fine structure (XAFS) is a powerful probe of local atomic structures, which is especially effective to study the local structures around dopants because of its elemental sensitivity.

In this work, Cr-, Co-, Ni-, and Cu-doped Bi_2Se_3 crystals are studied. Bi_2Se_3 is used as a parent crystal for its relatively large band gap among the TIs, which makes Bi_2Se_3 suitable for room-temperature applications. X-ray diffraction (XRD) and extended XAFS (EXAFS) experiments are performed to examine the local structures around the dopants. The nearest neighbors of the dopants are Se atoms for all samples and the X-Se bond lengths are extracted by EXAFS fitting procedures. The relaxed local structures around the Bi substitutional site

*zyang@fudan.edu.cn
†qiaoshan@fudan.edu.cn

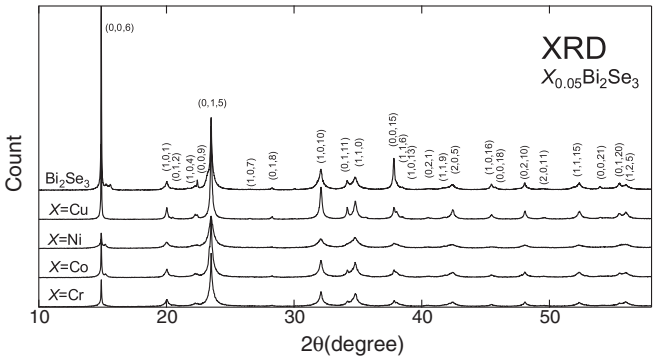

FIG. 1. The XRD patterns of $X_{0.05}Bi_2Se_3$ (X = Cr, Co, Ni, and Cu) and undoped Bi_2Se_3. The labels on the peaks are indices of the crystal planes in Bi_2Se_3.

and the intercalated site for X-doped Bi_2Se_3 are obtained from first-principles calculations and compared with our EXAFS results to judge the occupied sites of the 3d dopants. Cr and Cu are found to take Bi substitutional sites. Co atoms may substitute Bi atoms or form Co_3Se_4 ($C2/m$) clusters while small clusters of Ni_3Se_4 ($C2/m$) are formed in $Ni_{0.05}Bi_2Se_3$.

II. METHODS

$X_{0.05}Bi_2Se_3$ (X = Cr, Co, Ni, and Cu) single crystals were grown via a two-step melting process. First, stoichiometric amounts of high-purity elements Bi (99.999%) and Se (99.999%) were melted in evacuated quartz tubes at 800 °C for 16 h, followed by furnace cooling to room temperature. Second, the stoichiometric amounts of transition metal X and pure Bi_2Se_3 crystal were sealed into evacuated quartz tube again. The materials were heated at 800 °C for 19 h followed by slow cooling to 550 °C over 2 days and annealing at 550 °C for 3 days. Then, the crystals were furnace cooled to room temperature. Another one-step melting process was also used through which $X_{0.05}Bi_2Se_3$ crystals were prepared directly from stoichiometric amounts of Bi, Se, and X. No detectable differences were found in EXAFS data of $X_{0.05}Bi_2Se_3$ crystals grown by the two different processes. All the samples have metallic sheen and can be cleaved very easily along the basal plane.

The XRD experiments were carried out in room temperature with powder samples, which were made from high-quality single-crystal pieces. The XRD experiments were done at Beamline 14B1 of Shanghai Synchrotron Radiation Facility (SSRF) with wavelength 1.2385 Å. The single crystals were ground up to powders just before the XRD experiments. To get the lattice constants precisely, two steps are taken to process the data. First, the locations of peaks are determined by profile fittings, and then the lattice constants are extracted from refined XRD patterns. The profile fittings are done with linear background in segments, in which Pearson-VII function is used and skewness is set to be zero. The observed locations are used in the cell refinement after the weak and strongly overlapped peaks are excluded.

The XRD patterns of $X_{0.05}Bi_2Se_3$ (X = Cr, Co, Ni, and Cu) are shown in Fig. 1. All the peaks can be labeled as Miller indices of Bi_2Se_3, suggesting that no additional phase forms in

TABLE I. The lattice constants of the samples extracted from XRD patterns.

Sample	a (Å)	c (Å)
Bi_2Se_3	4.142 ± 0.001	28.660 ± 0.003
$Cr_{0.05}Bi_2Se_3$	4.141 ± 0.003	28.66 ± 0.02
$Co_{0.05}Bi_2Se_3$	4.142 ± 0.001	28.645 ± 0.007
$Ni_{0.05}Bi_2Se_3$	4.141 ± 0.006	28.68 ± 0.03
$Cu_{0.05}Bi_2Se_3$	4.140 ± 0.001	28.654 ± 0.004

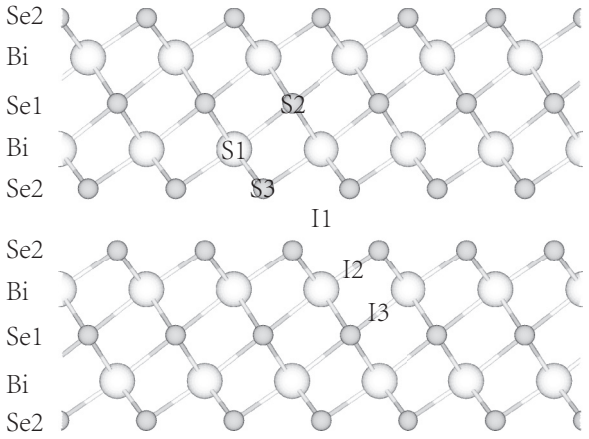

FIG. 2. Side view of the crystal structure of Bi_2Se_3 and the six high-symmetry sites, labeled as S1, S2, S3, I1, I2, and I3, respectively. The coordinations of the six sites are shown in Table II.

TABLE II. The initial environment around the six high-symmetry sites in Bi_2Se_3 ($R\bar{3}m$) crystal with the lattice constants $a = b =$ 4.140 Å and $c = 28.636$ Å. The coordination numbers and element are shown in brackets.

Site	First shell (Å)	Second shell (Å)	Third shell (Å)
S1	2.89(3Se)	4.14(6Bi)	4.80(3Se)
(0, 0, 0.399)	3.04(3Se)	4.46(3Bi)	5.05(3Se)
			5.14(3Se)
S2	3.04(6Bi)	4.14(6Se)	5.14(6Bi)
(0, 0, 0)		4.24(6Se)	
S3	2.89(3Bi)	4.14(6Se)	4.80(3Bi)
(0, 0, 0.208)	3.49(3Se)	4.24(3Se)	5.05(3Bi)
			5.38(1Bi)
			5.41(3Se)
I1	2.71(6Se)	2.89(2Bi)	4.95(6Se)
(0, 0, 0.5)			5.05(12Bi)
			5.34(6Se)
I2	2.52(3Se3Bi)	3.35(1Se)	4.85(3Se3Bi)
(2/3, 1/3, 0.427)	2.69(1Se)		4.94(6Se)
			5.16(3Bi)
			5.33(3Se)
I3	2.57(4Se3Bi)	2.82(1Bi)	4.87(9Se3Bi)
(1/3, 2/3, 0.366)			5.01(6Bi)
			5.04(3Se)

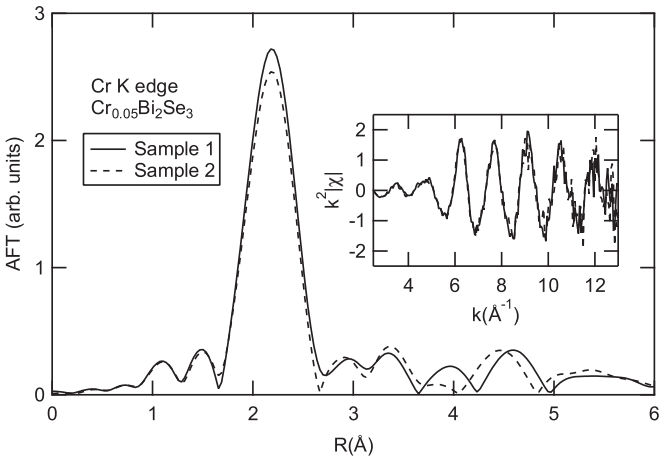

FIG. 3. The AFTs of $k^2\chi(k)$ (inset) of two $Cr_{0.05}Bi_2Se_3$ samples.

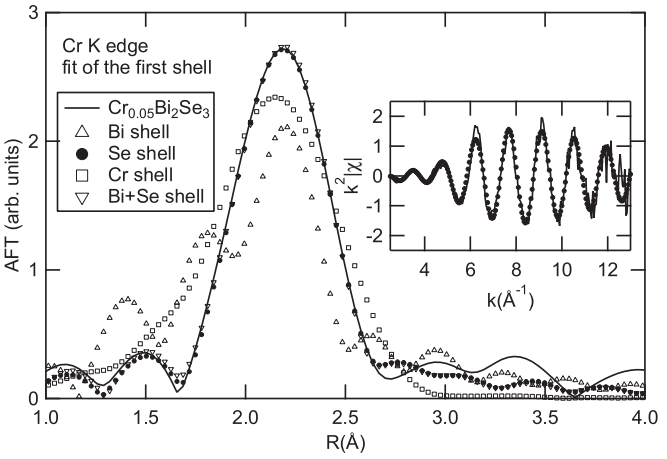

FIG. 4. The AFTs of $Cr_{0.05}Bi_2Se_3$ and the first shell fittings with the Se shell, Bi shell, Cr shell, and Bi-Se mixed shell. The inset shows $k^2\chi(k)$ of $Cr_{0.05}Bi_2Se_3$ and the fitting with the Se shell.

these samples. However, the XRD patterns can only reflect the long-range order in the crystals, so the absence of additional peaks can not rule out the existence of small clusters in the samples. Supposing hexagonal lattices, the lattice constants a and c of the four samples are extracted from XRD patterns as shown in Table I. The lattice constant a is almost the same for all samples. The lattice constant c is unchanged for Cr dopants and changed for Co, Ni, and Cu dopants compared with undoped Bi_2Se_3. It decreases by 0.05% for Co dopants, increases by 0.07% for Ni dopants, and decreases by 0.02% for Cu dopants.

The EXAFS experiments were performed in room temperature also with powder samples from high-quality single-crystal pieces. Since the concentration of X (X = Cr, Co, Ni, and Cu) in these samples is low, and Bi and Se are high-Z elements with large x-ray absorptions, it is difficult to do EXAFS measurements in transmission mode and the fluorescence one is used, by means of an 18-channel Silicon drift detector array in Beamline 1W1B of Beijing Synchrotron Radiation Facility (BSRF). The experiments were redid at Beamline 14W1 of SSRF to check the repeatability of the data. The ATHENA and ARTEMIS codes [27] are used for data processing and fitting, respectively.

To investigate the structure relaxation of the local structures around X in $X_{0.05}Bi_2Se_3$ (X = Cr, Co, Ni, and Cu), the first-principles calculations are performed. The calculations are conducted by the plane-wave method within the framework of density functional theory (DFT), as implemented in the VASP code [28]. Two combinations are used to rule out the divergence caused by the calculation, one of which is the projector-augmented wave pseudopotential with exchange-correlation function described by the generalized gradient approximation (PAW-GGA) [29] in the Perdew-Wang form [30] and the other is the ultrasoft pseudopotential with local density approximation (USPP-LDA) [29,31]. All of the calculations are carried with a plane-wave cutoff energy of 300 eV and the 5×5×1 Monkhorst-Pack k-point meshes. A 3×3×1 supercell containing 54 Bi atoms and 81 Se atoms is taken to minimize the interaction between the dopants. All atoms in the supercell are allowed to relax until the Hellmann-Feynman force on each atom is smaller than 0.01 eV/Å.

III. RESULTS AND DISCUSSION

The crystal structure of Bi_2Se_3 is shown in Fig. 2. Bi_2Se_3 has a layer-by-layer structure with periodical Se-Bi-Se-Bi-Se quintuple layers. The middle Se layer of each quintuple layer is labeled as Se1 and the other two Se layers are labeled as Se2. The coordinations and the first three shells of six high-symmetry sites in Bi_2Se_3, which have the relatively large space, are shown in Table II. There are three substitutional sites in Bi_2Se_3, i.e., the Bi substitutional site (S1), the Se1 substitutional site (S2), and the Se2 substitutional site (S3), and three high-symmetry interstitial sites, i.e., the hollow site between the two Se2 layers (I1), the hollow site between the Bi layer and the Se2 layer (I2), and the hollow site between the Bi layer and the Se1 layer (I3). These six sites are more likely taken by dopants because of the relatively large interstices

TABLE III. The structural parameters from the first shell fittings with the models.

Model	Pair	R (Å)	N	S_0^2	$\triangle E$ (eV)	σ^2 (Å^2)	R factor
Bi shell	Cr-Bi	2.21 ± 0.01	3 ± 2	0.66	-4 ± 4	0.000 ± 0.003	7%
Cr shell	Cr-Cr	2.54 ± 0.04	8	0.66	-16 ± 7	0.006 ± 0.002	6%
	Cr-Cr	2.93 ± 0.04	6	0.66	-16 ± 7	0.006 ± 0.002	
Se shell	Cr-Se	2.50 ± 0.01	6	0.66	-1 ± 1	0.0033 ± 0.0002	0.2%
Bi+Se shell	Cr-Bi	2.50 ± 0.01	6 ± 1	0.66	-25 ± 10	0.06 ± 0.04	0.2%
	Cr-Se	2.50 ± 0.01	6 ± 1	0.66	-1 ± 1	0.0036 ± 0.0007	

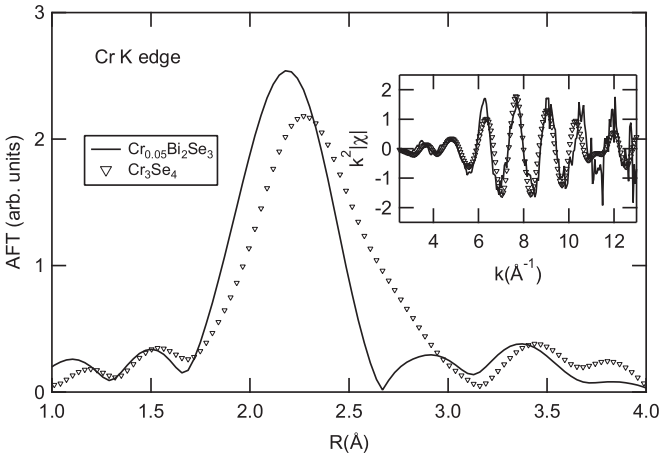

FIG. 5. The fitting with the structure of Cr_3Se_4.

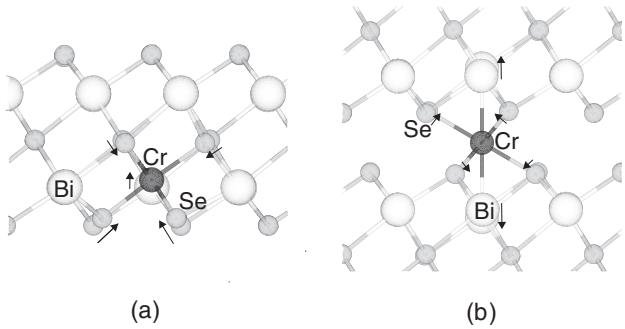

FIG. 6. Side view of the equilibrium local structures around Cr atoms occupying the (a) S1 site and (b) I1 site in Bi_2Se_3 crystal obtained from the first-principles calculation using PAW-GGA. The arrows denote the directions of the movements of the atoms from their initial positions.

around them. In this paper, only these six sites in Bi_2Se_3 are considered and judged.

The elements of the first shell can be distinguished by the fittings since different elements contribute different phase shifts and scattering amplitudes as functions of electron energy which modulate the EXAFS oscillations. In the data analysis below, clusters of the doped atoms are considered first. Then, the existence of X-Se (X = Cr, Co, Ni, and Cu) compounds is examined by comparing the extracted X-Se bond lengths in $X_{0.05}Bi_2Se_3$ samples with that in X-Se compounds. The first shell fittings with the Bi shell and Bi-Se mixed shell are performed to judge the occupancies of the six high-symmetry sites in Bi_2Se_3. The ratio of Bi to Se is set to 1 in the Bi-Se mixed shell because it is about 1 for S3, I2, and I3 sites and the other three sites have no mixed first shell, as shown in Table II. The S2, S3, I2, and I3 sites can be ruled out for all the samples by the first shell fittings. The equilibrium local structures around the dopants occupying S1 and I1 sites are obtained from the first-principles calculations to judge the occupancies of these two sites by comparing the equilibrium bond lengths with experimental results.

A. Local structures around Cr atoms in $Cr_{0.05}Bi_2Se_3$

The amplitudes of Fourier transform (AFT) of the weighted Cr K-edge EXAFS functions $k^2\chi(k)$ of two $Cr_{0.05}Bi_2Se_3$ samples are shown in Fig. 3. The EXAFS oscillations of them coincide well with each other, which confirms the repeatability of the data. A single strong peak locates at about 2.2 Å which should result from the first atomic shell around the Cr atoms.

To examine the existence of Cr clusters, the fitting of the first shell peak with the Cr shell is performed. The Cr crystal has a body-centered-cubic structure and the first Cr shell consists of two subshells with distances 2.49 and 2.88 Å and coordination numbers 8 and 6. In the fitting, S_0^2 of chromium is fixed to the theoretical value 0.66 [32] and coordination numbers of the two subshells are fixed as 8 and 6. The fitting result is shown in Fig. 4 and Table III. R factor denotes the figure of merit for the fit. The poor fit of the model of the Cr shell with a large-R factor, 6%, rules out the existence of Cr clusters in the sample.

The fittings of the first shell peak with the Bi shell, Se shell, and Bi-Se mixed shell are also performed as shown in Fig. 4 and Table III. In all of the fittings, S_0^2 of chromium is fixed to the theoretical value 0.66 [32]. In the fitting with the Bi-Se mixed shell, the distances and coordination numbers of Cr-Bi and Cr-Se paths are restricted to be the same as discussed before. In the fitting with the Se shell, the coordination number is fixed as 6 according to the coordination numbers of the first Se shell around S1 and I1 sites because only around these two sites the first shell is pure Se shell. The Bi shell gives a poor fit while the AFT curves of the fittings with the Se shell and the Bi-Se mixed shell almost coincide with each other. However, the Cr-Bi path of the Bi-Se mixed shell model has an extremely large σ^2 which greatly reduces the contribution of the Cr-Bi path and the parameters of the Cr-Se path of the Bi-Se mixed shell model are close to that of the Se shell model. These results demonstrate that the first shell around Cr atoms in $Cr_{0.05}Bi_2Se_3$ is the Se shell. The values obtained for ΔE_0, R, and σ^2 of the first Se shell are -1 ± 1 eV, 2.50 ± 0.01 Å, and 0.0033 ± 0.0002 Å^2, respectively. As shown in Table II, only S1 and I1 sites among the six sites that have the first Se shell while the first shells of other sites are the Bi shell and the Bi-Se mixed shell, so S2, S3, I2, and I3 sites can be ruled out.

The average Cr-Se bond lengths of CrSe ($P6_3mc$) [33], Cr_3Se_4 ($I2/m$), and Cr_7Se_8 ($C2/m$) [34] are 2.60, 2.54, and 2.62 Å, respectively, among which the Cr-Se bond length of Cr_3Se_4 ($I2/m$) is close to the experimental results. So, the fitting with the structure of Cr_3Se_4 ($I2/m$) is performed as

TABLE IV. The structural parameters of Cr_3Se_4 obtained from the fitting.

Model	Pair	R (Å)	N	S_0^2	$\triangle E$ (eV)	σ^2 (Å^2)	σ_S^2 (Å^2)	R factor
Cr_3Se_4	Cr-Se	2.54	6	0.8 ± 0.5	7 ± 2	0.002 ± 0.005	0.0033	4.4%
	Cr-Cr	3.19	10/3	0.8 ± 0.5	10 ± 6	0.002 ± 0.005	0.026	
	Cr-Cr	3.72	10/3	0.8 ± 0.5	10 ± 6	0.002 ± 0.005	0.019	

TABLE V. The first two shells around Cr atoms occupying the S1 and I1 sites obtained from the first-principles calculations using the two combinations. The distances are in Å.

	PAW-GGA		USPP-LDA	
Site	First shell	Second shell	First shell	Second shell
S1	2.57(3Se)	4.11(6Bi)	2.53(3Se)	4.11(6Bi)
	2.66(3Se)	4.28(3Bi)	2.61(3Se)	4.22(3Bi)
I1	2.66(6Se)	3.18(2Bi)	2.63(6Se)	3.17(2Bi)

shown in Fig. 5 and Table IV. Cr_3Se_4 ($I2/m$) has three shells below 4 Å which all consist of several subshells with different distances. σ_S^2 is the variance of the distances of subshells in a shell, which will reduce the EXAFS signals of the shell. The fitting result is displayed in Fig. 5, which obviously shows an unreasonable fitting, suggesting that most Cr atoms in $Cr_{0.05}Bi_2Se_3$ do not form Cr-Se compounds. So, only S1 and I1 sites are possible.

The equilibrium local structures around Cr atoms occupying the S1 and I1 sites in Bi_2Se_3 crystal are calculated by the first-principles calculations using PAW-GGA, as shown in Fig. 6 and the distances of the first two shells are shown in Table V. The six nearest Se atoms around the Cr dopant move towards the Cr dopant while further atoms do not move distinctly. Although the initial Cr-Se bond length on the S1 site is much longer than that on the I1 site, the equilibrium value on the S1 site is shorter than that on the I1 site, which should be attributed to the stronger bonding of Cr and Se when Cr takes the S1 site. Since the equilibrium Cr-Se bond length on S1 site is closer to experimental results, Cr should take the S1 site rather than the I1 site.

The 2.50-Å experimental bond length is 0.12 Å smaller than the 2.62-Å average equilibrium Cr-Se bond length around S1. It may originate from the factors which are not considered in the theoretical models. So, we recalculate the equilibrium local structures using USPP-LDA and the distances of the first two shells are shown in Table V. The average equilibrium Cr-Se bond lengths obtained using USPP-LDA are 2.57 Å for the S1 site and 2.63 Å for the I1 site. The precise

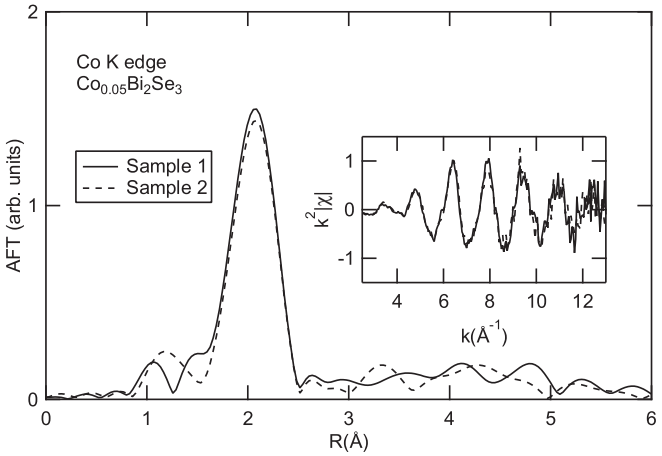

FIG. 7. The AFTs of $k^2\chi(k)$ (inset) of two $Co_{0.05}Bi_2Se_3$ samples.

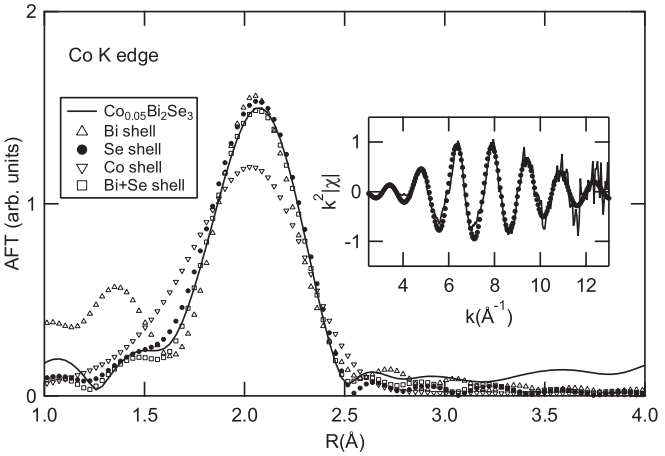

FIG. 8. The AFTs of $Co_{0.05}Bi_2Se_3$ and the first shell fittings with Se shell, Bi shell, Co shell, and Bi-Se mixed shell. The inset shows $k^2\chi(k)$ of $Co_{0.05}Bi_2Se_3$ and the fitting with the Se shell.

values of the distances slightly differ from those obtained using PAW-GGA, but the qualitative results remain that the average equilibrium Cr-Se bond length for the S1 site is smaller than that for the I1 site. The results obtained using USPP-LDA are closer to the experimental ones than those using PAW-GGA, which may due to that the USPP potential includes more electronic states into the calculations. The theoretical studies of Cr substituting Bi atoms in Bi_2Se_3 have been reported using PAW potential and the Perdew-Burke-Ernzenhof generalized gradient approximation (PBE-GGA) for the exchange-correlation function [25] whose results of the average Cr-Se bond lengths, 2.60 Å, are well consistent with our theoretical results shown in Table V.

The theoretical bond lengths can have quantitatively slight deviations from the real case, but the qualitative results obtained from the theoretical calculations are reliable so that the structure relaxation around S1 is stronger than that around I1, and this consideration is the base to judge the occupied site. So, the inclination between S1 and I1 sites can be judged

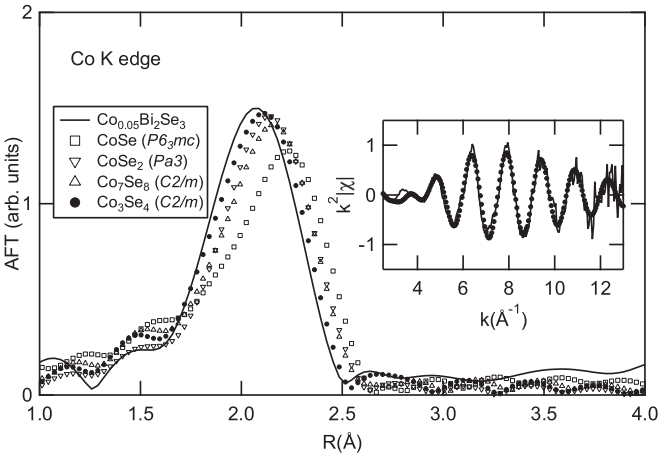

FIG. 9. The AFTs of $Co_{0.05}Bi_2Se_3$ and the first shell fittings with Co-Se compounds.

TABLE VI. The structural parameters obtained from the first shell fittings with the models.

Model	Pair	R (Å)	N	S_0^2	$\triangle E$ (eV)	σ^2 (Å^2)	R factor
Bi shell	Co-Bi	2.33 ± 0.01	10 ± 1	0.69	-46 ± 2	0.007 ± 0.001	0.4%
Co shell	Co-Co	2.48 ± 0.06	12	0.69	-5 ± 8	0.018 ± 0.005	28%
Se shell	Co-Se	2.40 ± 0.01	6	0.69	-4 ± 2	0.0086 ± 0.0004	0.9%
Bi+Se shell	Co-Bi	2.40 ± 0.01	4 ± 1	0.69	0 ± 12	0.2 ± 0.1	0.1%
	Co-Se	2.40 ± 0.01	4 ± 1	0.69	-4 ± 1	0.0056 ± 0.0004	

by comparing the theoretical and experimental Cr-Se bond lengths.

In addition, the first Se shell of Cr occupying S1 site splits into two Se subshells separated from each other by 0.08 Å for USPP-LDA. The distance differences of 0.08 Å can contribute to the Debye-Waller factor by about 0.003 Å^2, so the Debye-Waller factors of the first shells of the samples should be larger than 0.003 Å^2. For the Cr-doped sample, it is only 0.0033 Å^2. Considering the contributions of temperature, the Debye-Waller factor should be larger. This fact may indicate that Cr does not occupy the S1 site or the theoretical results using USPP-LDA still have slight deviations in quantity. But, as stated in the beginning, this work only restricts the discussions to the six high-symmetry sites. The experimental results only tell us that S1 is more possibly occupied than the other five high-symmetry sites.

B. Local structures around Co atoms in $Co_{0.05}Bi_2Se_3$

The AFTs of Co K-edge EXAFS function $k^2\chi(k)$ of two $Co_{0.05}Bi_2Se_3$ samples are shown in Fig. 7. The k range in Fourier transform is from 2 to 13 Å^{-1}. The coincidence of the EXAFS oscillations of them demonstrates the repeatability of the data within about 3 Å in R space. Only the first shell peak can be recognized and the signals of further shells are obscured by the statistical errors.

The existence of Co clusters can be ruled out by the bad fitting of the first shell peak with the Co shell, which is shown in Fig. 8 and Table VI. During the fitting, the coordination number of the Co shell is fixed as 12 which is that of the first shell in Co metal and S_0^2 of cobalt is fixed as the theoretical value 0.69 [32].

As shown in Fig. 8, the first shell fittings with the Se shell, Bi shell and Bi-Se mixed shell are also performed and the obtained parameters are shown in Table VI. Obviously, only the Se shell can give a reasonable fit while neither the Bi shell nor the Bi-Se mixed shell gets reasonable parameters from the fittings. The values obtained for ΔE_0, R, and σ^2 of the Se shell are -4 ± 2 eV, 2.40 ± 0.01 Å, and 0.0086 ± 0.0004, respectively. Only the S1 site, I1 site, and Co-Se compounds should be considered.

The average Co-Se bond lengths of CoSe ($P6_3mc$) [33], $CoSe_2$ ($Pa3$) [35], Co_7Se_8 ($C2/m$), and Co_3Se_4 ($C2/m$) [36] are 2.48, 2.44, 2.46, and 2.45 Å, respectively. None of them are consistent with the experimental results but the differences are not large. So, the fittings of the first shell peak with structures of the four Co-Se compounds are performed as shown in Fig. 9 and Table VII. Co_3Se_4 ($C2/m$) gives the best fit among the four Co-Se compounds which is possibly the case for the Co atoms in $Co_{0.05}Bi_2Se_3$.

Then, we consider the S1 and I1 sites. Figure 10 shows the relaxed local structures around Co atoms occupying the S1 and I1 sites obtained from the first-principles calculations using PAW-GGA. The equilibrium distances of the first two shells obtained using the two combinations are shown in Table VIII. The relaxations of the local structures around Co atoms are similar to that around Cr atoms. The average equilibrium Co-Se bond lengths on the S1 and I1 sites are 2.48 and 2.61 Å using PAW-GGA, and 2.42 and 2.56 Å using USPP-LDA, respectively. Since the experimental Co-Se bond length, 2.40 Å, is closer to that of the S1 site for both theoretical results, Co should also take the S1 site rather than the I1 site in $Co_{0.05}Bi_2Se_3$. So, Co dopants may either take the S1 site or form Co_3Se_4 ($C2/m$) clusters which can not be distinguished by EXAFS analysis.

C. Local structures around Ni atoms in $Ni_{0.05}Bi_2Se_3$

Figure 11 shows the AFTs of the weighted Ni K-edge EXAFS functions $k^2\chi(k)$ of two $Ni_{0.05}Bi_2Se_3$ samples. The coincidence of them indicates the repeatability of the data. The first shell peak locates at about 2.1 Å, and three other shells can be recognized at about 2.8, 3.4, and 4.1 Å.

The same as Cr- and Co-doped samples, the fittings of the first shell peak with the Ni shell model are performed, as shown in Fig. 12 and Table IX. Ni has a face-centered-cubic lattice

TABLE VII. The structural parameters of the Co-Se compounds obtained from the fittings.

Compound	Pair	R (Å)	N	S_0^2	δE (eV)	σ^2 (Å^2)	σ_S^2 (Å^2)	R factor
CoSe ($P6_3mmc$)	Co-Se	2.48	6	0.69	13 ± 4	0.008 ± 0.003		8.5%
	Co-Co	2.65	2	0.69	1 ± 10	0.01 ± 0.02		
$CoSe_2$ ($Pa3$)	Co-Se	2.44	6	0.69	4 ± 1	0.0086 ± 0.0006		2.4%
Co_3Se_4 ($C2/m$)	Co-Se	2.45	6	0.69	6 ± 1	0.0027 ± 0.0003	0.0033	0.5%
	Co-Co	2.68	4/3	0.69	-2 ± 2	0.0027 ± 0.0003		
Co_7Se_8 ($C2/m$)	Co-Se	2.46	6	0.69	9 ± 2	0.0044 ± 0.0007	0.0028	2.4%
	Co-Co	2.68	12/7	0.69	0 ± 6	0.0044 ± 0.0007	0.0038	

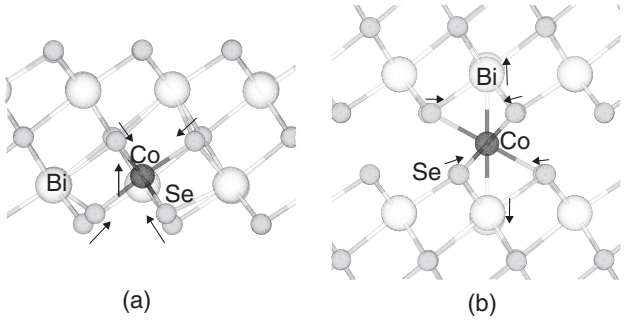

FIG. 10. Side view of the equilibrium local structures around Co atoms occupying the (a) S1 site and (b) I1 site in Bi_2Se_3 crystal obtained by the first-principles calculations using PAW-GGA. The arrows denote the directions of the movements of the atoms from their initial positions.

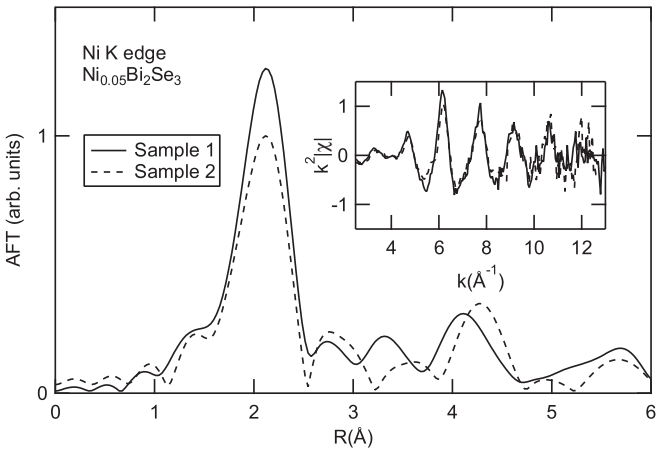

FIG. 11. The AFTs of $k^2\chi(k)$ (inset) of two $Ni_{0.05}Bi_2Se_3$ samples.

and the coordination number of the first Ni shell is 12. During the fitting, S_0^2 is fixed as the theoretical value 0.69 [32] and the coordination number is fixed as 12. The bad fitting with a large-R factor, 12%, rules out the existence of Ni clusters.

The first shell fittings with the Se shell, Bi shell, and Bi-Se mixed shell are shown in Fig. 12 and Table IX. The fitting procedures are similar to those of $Cr_{0.05}Bi_2Se_3$ and the results also show that only the Se shell fits the first shell peak reasonably, which demonstrates that the nearest neighbors of Ni atoms are Se atoms. The values obtained for ΔE_0, R, and σ^2 of the first Se shell are -5 ± 2 eV, 2.46 ± 0.01 Å, and 0.0096 ± 0.0004, respectively.

The average Ni-Se bond lengths of NiSe ($P6_3mc$) [33], $NiSe_2$ ($Pa3$) [35], Ni_3Se_2 ($R32$), and Ni_3Se_4 ($C2/m$) [37] are 2.50, 2.49, 2.39, and 2.46 Å, respectively, among which Ni_3Se_4 ($C2/m$) is well consistent with the experimental results. The fitting with the local structure around Ni atoms in Ni_3Se_4 ($C2/m$) is performed, as shown in Fig. 13 and Table X. Ni_3Se_4 ($C2/m$) fits the first shell peak quite well and the three distant peaks are also reasonable. This indicates that Ni_3Se_4 ($C2/m$) clusters may be formed in $Ni_{0.05}Bi_2Se_3$. Since no x-ray diffraction peaks of Ni_3Se_4 ($C2/m$) appear in the XRD pattern of $Ni_{0.05}Bi_2Se_3$, the sizes of clusters should be small.

Then, we consider the possibility of occupancy of the six sites in Bi_2Se_3 shown in Fig. 2 and Table II. The S2, S3, I2, and I3 sites are all ruled out by the results of the first shell fittings and only the S1 and I1 sites are possible. The relaxed local structures around Ni atoms occupying S1 and I1 sites are also calculated by the first-principles calculations using the two combinations, as shown in Fig. 14 and Table XI. Both results of them show that once Ni atom substitutes Bi, the six nearest Se atoms move closer while the further atoms do not move distinctly, which is similar to Cr- and Co-doped samples. The equilibrium Ni-Se bond length on the S1 site is closer to the experimental results than that on the I1 site, so the possibility of the I1 site can be ruled out. However, the distances of the second Bi shell around the Ni atom occupying the S1 site are over 4.1 Å, which can not contribute the peaks at 2.8 and 3.4 Å in AFT of $Ni_{0.05}Bi_2Se_3$. These results rule out the S1 and I1 sites, and Ni_3Se_4 ($C2/m$) clusters should be the case for Ni atoms in $Ni_{0.05}Bi_2Se_3$.

TABLE VIII. The first two shells around Co atoms occupying the S1 and I1 sites obtained from the first-principles calculations using the two combinations. The distances are in Å.

	GGA		USPP-LDA	
Site	First shell	Second shell	First Shell	Second Shell
S1	2.44(3Se)	4.11(6Bi)	2.39(3Se)	4.11(6Bi)
	2.53(3Se)	4.22(3Bi)	2.46(3Se)	4.16(3Bi)
I1	2.61(6Se)	3.02(2Bi)	2.56(6Se)	3.02(2Bi)

D. Local structures around Cu atoms in $Cu_{0.05}Bi_2Se_3$

Figure 15 shows the AFTs of the weighted Cu K-edge EXAFS functions $k^2\chi(k)$ of two $Cu_{0.05}Bi_2Se_3$ samples. Although the statistical error of sample 2 is much larger than that of sample 1, the coincidence of the EXAFS oscillations of them can still be recognized. Compared to the AFTs of them, the coincidence remains below 3.0 Å. The first shell peak locates at about 2.1 Å.

Same as Cr-, Co-, and Ni-doped samples, the existence of Cu clusters can be ruled out by the bad fitting of the first shell

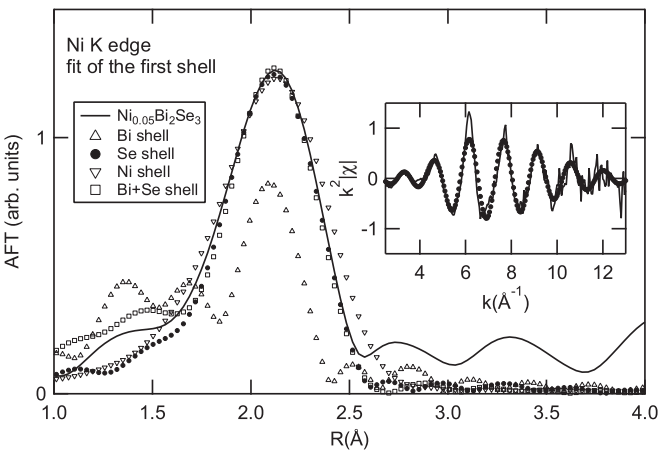

FIG. 12. The AFTs of $Ni_{0.05}Bi_2Se_3$ and the first shell fittings with Se shell, Bi shell, Ni shell, and Bi-Se mixed shell. The inset shows $k^2\chi(k)$ of $Ni_{0.05}Bi_2Se_3$ and the fitting with the Se shell.

TABLE IX. The structural parameters obtained from the first shell fittings with the models.

Model	Pair	R (Å)	N	S_0^2	ΔE (eV)	σ^2 (Å^2)	R factor
Bi shell	Ni-Bi	2.14 ± 0.03	2 ± 2	0.69	-10 ± 6	0.005 ± 0.005	31%
Ni shell	Ni-Ni	2.55 ± 0.03	12	0.69	-4 ± 4	0.017 ± 0.002	12%
Se shell	Ni-Se	2.46 ± 0.01	6	0.69	-5 ± 2	0.0096 ± 0.0004	0.9%
Bi+Se shell	Ni-Ni	2.43 ± 0.01	5 ± 1	0.69	36 ± 4	0.011 ± 0.002	1.6%
	Ni-Se	2.43 ± 0.01	5 ± 1	0.69	-8 ± 3	0.011 ± 0.002	

peak with the Cu shell, as shown in Fig. 16 and Table XII. The fittings of the first shell peak are also performed with the Se shell, Bi shell, and Bi-Se-mixed shell, as shown in Fig. 16. The fitting procedures are similar to those of $Cr_{0.05}Bi_2Se_3$. S_0^2 of copper is fixed as theoretical value 0.70 [32]. Again, only the Se shell gives a reasonable fit while neither the Bi shell nor the Bi-Se mixed shell does, which demonstrates that Se atoms are the nearest neighbors of Cu atoms in $Cu_{0.05}Bi_2Se_3$. The values obtained for ΔE_0, R, and σ^2 of the Se shell are -1 ± 4 eV, 2.39 ± 0.02 Å, and 0.012 ± 0.001, respectively.

The average Cu-Se bond lengths of CuSe ($P6_3/mmc$) [38], $CuSe_2$ ($Pa3$), Cu_3Se_2 ($P\bar{4}2_1m$) [39], $CuSe_2$ ($Pnnm$) [40], and Cu_2Se ($Fm3m$) [41] are 2.27, 2.57, 2.46, 2.56, and 2.50 Å, respectively, none of which are consistent with experimental results, indicating that none of them form in $Cu_{0.05}Bi_2Se_3$.

The equilibrium local structures around Cu atoms occupying the S1 and I1 sites are also calculated using the two combinations, as shown in Fig. 17 and Table XIII. Both results of them show that the local structures around Cu atoms occupying the I1 site are similar to those around Cr, Co, and Ni dopants while those around Cu atoms occupying the S1 site are quite different from those around other dopants. For Cr, Co, and Ni atoms occupying the S1 site, the doped atoms move slightly towards the Se1 layer and the six nearest Se atoms move towards the dopants distinctly. However, for Cu atoms occupying the S1 site, the six nearest Se atoms around the S1 site hardly move and the Cu dopants move towards the Se2 layer dramatically. The movement of Cu dopants reduces the Cu-Se bond length on the S1 site to 2.38 Å using PAW-GGA and to 2.34 Å using USPP-LDA, which is well consistent with the experimental results. The coordination number of the first Se shell changes to 3, so the first shell fitting is performed again with coordination number fixed as 3. The values obtained for ΔE_0, R, and σ^2 of the first Se shell are -2 ± 2 eV, 2.38 ± 0.01 Å, and 0.0069 ± 0.0004, respectively. The Cu-Se bond length remains consistent with the experimental results, so the Cu atoms should take the S1 site.

E. Discussion

As summarized in Table XIV, from our results, Cr and Cu dopants mostly substitute Bi atoms in Bi_2Se_3, which differs from several reported experimental results. Although the theoretical researches report that Cr is more stable at the Bi substitutional site [24,25], Cr dopants are found occupying both the Bi substitutional sites and the interstitial sites in the Cr-doped Bi_2Se_3 grown by the molecular beam epitaxy method [16]. Cu dopants are restricted into the vdW gap in Bi_2Se_3 by the electrochemical intercalation technique [7], while Cu dopants may either intercalate into the vdW gap or randomly substitute Bi atoms in Cu-doped Bi_2Se_3 grown through a process of heating and quenching [8]. These differences result from the dependence of the site occupancy on the sample growing process. Since the ideal growing condition assumed in the theoretical studies may not be achievable in experiments, metastable sites may be preferred during specific growing processes. This provides extra flexibility for manipulating the site occupancy of 3d dopants by growing processes.

The X-Se bond lengths extracted from the EXAFS are smaller than the initial Bi-Se bond lengths in Bi_2Se_3, which shows the direct evidence of structural relaxation around

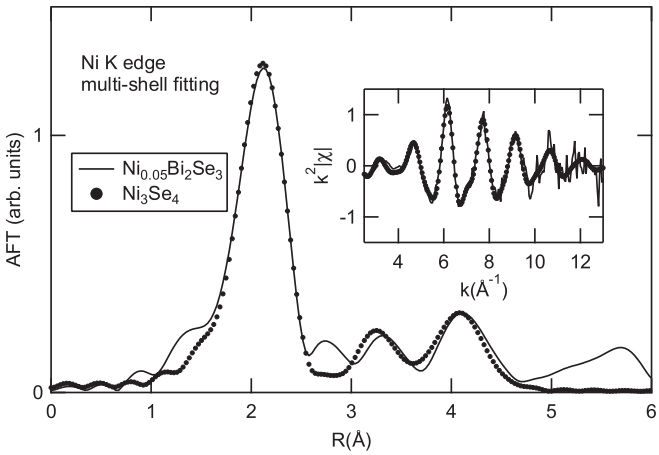

FIG. 13. The AFTs of $k^2\chi(k)$ (inset) of $Ni_{0.05}Bi_2Se_3$ and the fittings with Ni_3Se_4.

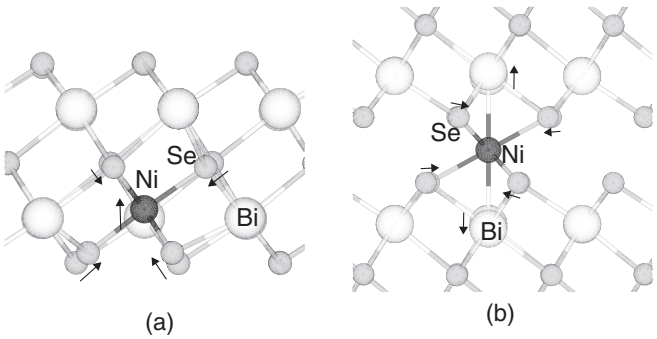

FIG. 14. Side view of the equilibrium local structures around Ni atoms occupying the (a) S1 site and (b) I1 site in Bi_2Se_3 crystal obtained by the first-principles calculations using PAW-GGA. The arrows denote the directions of the movements of the atoms from their initial positions.

TABLE X. The structural parameters of Ni_3Se_4 obtained from the fitting.

Model	Pair	R(Å)	N	S_0^2	ΔE	σ^2(Å^2)	σ_S^2(Å^2)	R factor
Ni_3Se_4 ($C2/m$)	Ni-Se	2.45 ± 0.01	6	0.63 ± 0.06	-5 ± 1	0.009 ± 0.001	0.0001	0.7%
	Ni-Ni	2.60 ± 0.01	4/3	0.63 ± 0.06	1 ± 1	0.009 ± 0.001		
	Ni-Ni	3.64 ± 0.02	14/3	0.63 ± 0.06	1 ± 1	0.014 ± 0.002	0.0004	
	Ni-Se	4.46 ± 0.01	12	0.63 ± 0.06	-5 ± 1	0.014 ± 0.002	0.0017	
	Ni-Ni	4.51 ± 0.01	8	0.63 ± 0.06	1 ± 1	0.014 ± 0.002	0.0003	

TABLE XI. The first two shells around the Ni atoms occupying the S1 and I1 sites obtained from the first-principles calculations using the two combinations. The distances are in Å.

	GGA		USPP-LDA	
Site	First shell	Second shell	First shell	Second shell
S1	2.50(3Se)	4.11(6Bi)	2.44(3Se)	4.11(6Bi)
	2.62(3Se)	4.27(3Bi)	2.53(3Se)	4.17(3Bi)
I1	2.60(6Se)	3.01(2Bi)	2.56(6Se)	3.00(2Bi)

TABLE XII. The structural parameters obtained from the first shell fittings with the models.

Model	Pair	R (Å)	N	S_0^2	ΔE (eV)	σ^2 (Å^2)	R factor
Bi shell	Cu-Bi	2.30 ± 0.01	4 ± 1	0.70	-46 ± 4	0.006 ± 0.001	0.1%
Cu shell	Cu-Cu	2.44 ± 0.05	12	0.70	-10 ± 8	0.020 ± 0.004	33%
Se shell	Cu-Se	2.39 ± 0.02	6	0.70	-1 ± 4	0.012 ± 0.001	1.8%
Se shell (2)	Cu-Se	2.38 ± 0.01	3	0.70	-2 ± 2	0.0069 ± 0.0004	0.9%
Bi+Se shell	Cu-Bi	2.42 ± 0.02	1 ± 1	0.70	5 ± 3	0.004 ± 0.003	16%
	Cu-Se	2.42 ± 0.02	1 ± 1	0.70	3 ± 6	0.004 ± 0.003	

TABLE XIII. The first two shells around Cu atoms occupying the S1 and I1 sites obtained from the first-principles calculations using the two combinations. The distances are in Å.

	GGA		USPP-LDA	
Site	First shell	Second shell	First shell	Second shell
S1	2.38(3Se)	3.77(3Se)	2.34(3Se)	3.87(3Se)
		3.90(3Se)		3.89(3Se)
		4.19(6Bi)		4.21(6Bi)
I1	2.66(6Se)	3.08(2Bi)	2.64(6Se)	3.08(2Bi)

TABLE XIV. Summarization of the structural parameters of the first shell around X (X = Cr, Co, Ni, and Cu) in $X_{0.05}Bi_2Se_3$.

X	Site	Bond	N	R_1 (Å)	σ_1^2 (Å^2)
Cr	S1	Cr-Se	6	2.50 ± 0.01	0.0033 ± 0.0002
Co	S1 or	Co-Se	6	2.40 ± 0.01	0.0086 ± 0.0004
	Co_3Se_4 ($C2/m$)				
Ni	Ni_3Se_4 ($C2/m$)	Ni-Se	6	2.45 ± 0.01	0.009 ± 0.001
Cu	S1	Cu-Se	3	2.38 ± 0.01	0.0069 ± 0.0004

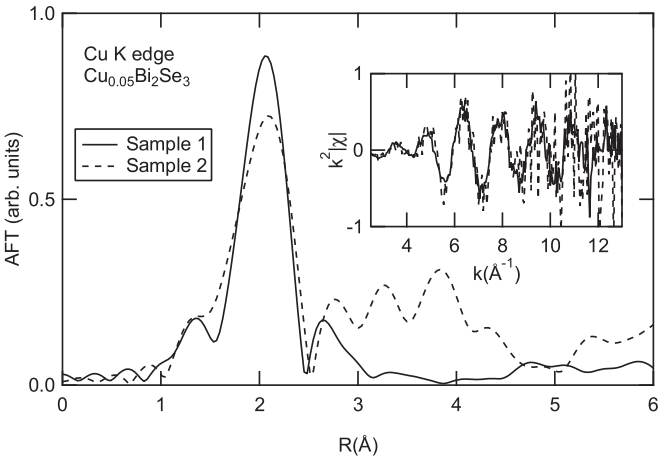

FIG. 15. The AFTs of $k^2\chi(k)$ (inset) of two $Cu_{0.05}Bi_2Se_3$ samples.

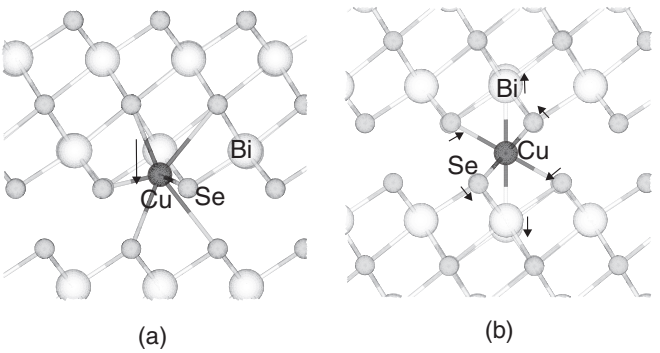

FIG. 17. Side view of the equilibrium local structures around Cu atoms occupying the (a) S1 site and (b) I1 site in Bi_2Se_3 crystal obtained by the first-principles calculations using PAW-GGA. The arrows denote the directions of the movements of the atoms from their initial positions.

dopants due to the smaller atomic sizes of 3*d* metal atoms than that of the Bi atom. The six Se atoms in the first shell around the S1 site must move towards the dopants once the Bi atom is substituted by a 3*d* metal atom. This structural relaxation should be responsible for the decrease of the lattice constants of the crystals and the *X*-Se bond lengths. The magnitude of the relaxation can be denoted by the decrease of the lattice constant *c* of the doped samples. The lattice constants *c* are 28.660 Å for undoped Bi_2Se_3, 28.66 Å for $Cr_{0.05}Bi_2Se_3$, 28.645 Å for $Co_{0.05}Bi_2Se_3$, and 28.654 Å for $Cu_{0.05}Bi_2Se_3$, indicating that the relaxation is the strongest for Co dopants and the weakest for Cr dopants among the three samples. The shorter bond length of Co-Se than that of Cr-Se should also be due to the stronger relaxation of the six Se atoms around Co dopants than that around Cr dopants. From our first-principles calculations, the shortest bond length of Cu-Se mainly results from the large shift of Cu atoms to the Se2 atomic layer, which does not happen for other dopants.

The magnitude of disorder of the first shell, denoted by the Debye-Waller factor σ^2, is found to be related to the magnitude of the relaxation. The Co-doped samples, which have the strongest relaxation, have the largest σ^2, 0.0086, among the Cr-, Co-, and Cu-doped samples. The Cr-doped samples, which have the weakest relaxation, have the smallest σ^2, 0.0033. The contrary to the law in $Ni_{0.05}Bi_2Se_3$ samples, which have the largest σ^2, 0.0096, and the largest lattice constant *c*, 28.68 Å, among the four doped samples, should result from the different environments around Ni atoms since Ni_3Se_4 ($C2/m$) clusters are formed.

Our EXAFS results show that the magnitude of structural relaxation increases with increasing atomic number for dopants from Cr to Co. The previous reported theoretical study of the site occupancy of 3*d* dopants in TIs suggests an energy-increasing tendency of substitutional cation site with increasing atomic number of dopants from V to Fe [26]. From the above two results, we can conclude that stronger structural relaxation results in higher formation energy.

Our theoretical average bond lengths of *X*-Se bond for the Bi substitutional site are 2.62 Å for Cr-Se and 2.48 Å for Co-Se using PAW-GGA, which is consistent with previous theoretical results which are 2.60 Å for Cr-Se and 2.49 Å for Co-Se using PAW and PBE-GGA [25]. Our other theoretical results using USPP-LDA, 2.57 Å for Cr-Se, and 2.42 Å for Co-Se are closer to the experimental ones, indicating that the USPP potential and LDA approximation describe the Cr- and Co-doped Bi_2Se_3 system more precisely than both above.

The local structures around 3*d* dopants can affect the atomic magnetic moments of them since the structural relaxation is closely related with the electronic structures through the hybridization between the host carriers and 3*d* electrons [42]. The local structural relaxations may also reduce the symmetry of the local structures, resulting in different occupancies of electronic states which are related to the local magnetic moments. Our results thus provide important information for the further study on the mechanism of magnetism in 3*d* doped TI systems.

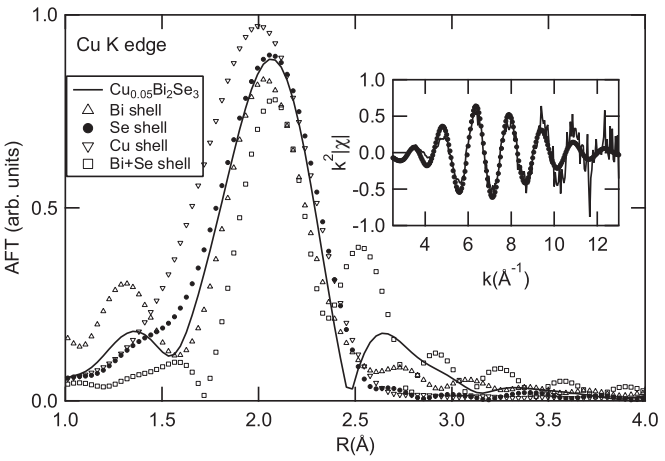

FIG. 16. The AFTs of $Cu_{0.05}Bi_2Se_3$ and the first shell fittings with the Se shell, Bi shell, Cu shell, and Bi-Se mixed shell. The inset shows $k^2\chi(k)$ of $Cu_{0.05}Bi_2Se_3$ and the fitting with the Se shell.

IV. CONCLUSION

In conclusion, we have studied the local structures around dopants in $X_{0.05}Bi_2Se_3$ (X = Cr, Co, Ni, and Cu) crystals by EXAFS experiments. Ni atoms in $Ni_{0.05}Bi_2Se_3$ form small Ni_3Se_4 ($C2/m$)clusters. Co atoms may substitute Bi atoms or form Co_3Se_4 ($C2/m$) clusters. Cr and Cu dopants substitute Bi atoms. The difference between site occupancy of the dopants in our samples and those reported before [7,8,16] shows its dependence on the sample growing process. The X-Se bond lengths are extracted from EXAFS fittings and give us direct evidence of structural relaxations around Cr, Co, and Cu dopants, among which it is strongest for Co dopants and weakest for Cr dopants. Our results also show that the higher disorder reflected by the larger Debye-Waller factor σ^2 relates with the stronger relaxation. The increasing structural relaxations from Cr to Co dopants discovered by our studies are consistent with the theoretical results reported before [26], which may contribute to the increasing formation energy of the substitutional Bi sites with increasing atomic number of dopants. Comparing the theoretical and experimental bond lengths, we find that the combination of USPP potential and LDA approximation describes Cr- and Co-doped Bi_2Se_3 systems more precisely than the PAW-GGA or PAW-PBE-GGA combination, indicating that potential and approximation should be properly chosen in further theoretical studies. The local structures around the magnetic dopants from our results supply basic information to the further studies on the mechanism of magnetisms in the magnetic doped Bi_2Se_3.

ACKNOWLEDGMENTS

We acknowledge the technical support and help from staff members of BL14B1 and BL14W1 beamline in SSRF and Beamline 1W1B in BSRF during the XRD and EXAFS measurements, and we also acknowledge the valuable discussions with Professor S. Wei of National Synchrotron Radiation Laboratory, University of Science and Technology of China. This work is supported by the Natural Science Foundation of China (Grants No. 10979021, No. 11027401, No. 11174054, No. 11304338, No. 11227902, and No. 61171011), the 973 project under Grant No. 2011CB921803, the Ministry of Science and Technology of China (National Basic Research Program No. 2011CB921800) and the "Strategic Priority Research Program(B)" of the Chinese Academy of Sciences (Grant No. XDB04010100).

[1] L. Fu and C. L. Kane, Phys. Rev. B **76**, 045302 (2007).
[2] H.-J. Zhang, C.-X. Liu, X.-L. Qi, X. Dai, Z. Fang, and S.-C. Zhang, Nat. Phys. **5**, 438 (2009).
[3] D. Hsieh, D. Qian, L. Wray, Y. Xia, Y. S. Hor, R. J. Cava, and M. Z. Hasan, Nature (London) **452**, 970 (2008).
[4] A. A. Taskin and Y. Ando, Phys. Rev. B **80**, 085303 (2009).
[5] A. Nishide, A. A. Taskin, Y. Takeichi, T. Okuda, A. Kakizaki, T. Hirahara, K. Nakatsuji, F. Komori, Y. Ando, and I. Matsuda, Phys. Rev. B **81**, 041309 (2010).
[6] Y. L. Chen, J. G. Analytis, J.-H. Chu, Z. K. Liu, S.-K. Mo, X. L. Qi, H. J. Zhang, D. H. Lu, X. Dai, Z. Fang, S. C. Zhang, I. R. Fisher, Z. Hussain, and Z.-X. Shen, Science **325**, 178 (2009).
[7] M. Kriener, Kouji Segawa, Zhi Ren, Satoshi Sasaki, Shohei Wada, Susumu Kuwabata, and Yoichi Ando, Phys. Rev. B **84**, 054513 (2011).
[8] Y. S. Hor, A. J. Williams, J. G. Checkelsky, P. Roushan, J. Seo, Q. Xu, H. W. Zandbergen, A. Yazdani, N. P. Ong, and R. J. Cava, Phys. Rev. Lett. **104**, 057001 (2010).
[9] Rui Yu, Wei Zhang, Hai-jun Zhang, Shou-Cheng Zhang, Xi Dai, and Zhong Fang, Science **329**, 61 (2010).
[10] Wang-Kong Tse and A. H. MacDonald, Phys. Rev. B **82**, 161104 (2010).
[11] Xiao-Liang Qi, Rundong Li, Jiadong Zang, and Shou-Cheng Zhang, Science **323**, 1184 (2009).
[12] Y. S. Hor, P. Roushan, H. Beidenkopf, J. Seo, D. Qu, J. G. Checkelsky, L. A. Wray, D. Hsieh, Y. Xia, S.-Y. Xu, D. Qian, M. Z. Hasan, N. P. Ong, A. Yazdani, and R. J. Cava, Phys. Rev. B **81**, 195203 (2010).
[13] Cui-Zu Chang, Jinsong Zhang, Minhao Liu, Zuocheng Zhang, Xiao Feng, Kang Li, Li-Li Wang, Xi Chen, Xi Dai, Zhong Fang, Xiao-Liang Qi, Shou-Cheng Zhang, Yayu Wang, Ke He, Xu-Cun Ma, and Qi-Kun Xue, Adv. Mater. **25**, 1065 (2013).
[14] Z. Salman, E. Pomjakushina, V. Pomjakushin, A. Kanigel, K. Chashka, K. Conder, E. Morenzoni, T. Prokscha, K. Sedlak, and A. Suter, arXiv:1203.4850.
[15] V. A. Kulbachinskii, A. Yu. Kaminskii, K. Kindo, Y. Narumi, K. Suga, P. Lostak, and P. Svanda, Phys. Lett. A **285**, 173 (2001).
[16] P. P. J. Haazen, J.-B. Laloe, T. J. Nummy, H. J. M. Swagten, P. Jarlllo-Herrero, D. Helman, and J. S. Moodera, Appl. Phys. Lett. **100**, 082404 (2012).
[17] L. Andrew Wray, Nat. Phys. **7**, 32 (2010).
[18] Joseph G. Checkelsky, Jianting Ye, Yoshinori Onose, Yoshihiro Lwasa, and Yoshinori Tokura, Nat. Phys. **8**, 729 (2012).
[19] D. Zhang, A. Richardella, D. W. Rench, S.-Y. Xu, A. Kandala, T. C. Flanagan, H. Beidenkopf, A. L. Yeats, B. B. Buckley, P. V. Klimov, D. D. Awschalom, A. Yazdani, P. Schiffer, M. Z. Hasan, and N. Samarth, Phys. Rev. B **86**, 205127 (2012).
[20] Cui-Zu Chang, Jinsong Zhang, Xiao Feng, Jie Shen, Zuocheng Zhang, Minghua Guo, Kang Li, Yunbo Ou, Pang Wei, Li-Li Wang, Zhong-Qing Ji, Yang Feng, Shuaihua Ji, Xi Chen, Jinfeng Jia, Xi Dai, Zhong Fang, Shou-Cheng Zhang, Ke He, Yayu Wang, Li Lu, Xu-Cun Ma, and Qi-Kun Xue, Science **340**, 167 (2013).
[21] Yi-Lin Wang, Yong Xu, Ye-Ping Jiang, Jun-Wei Liu, Cui-Zu Chang, Mu Chen, Zhi Li, Can-Li Song, Li-Li Wang, Ke He, Xi Chen, Wen-Hui Duan, Qi-Kun Xue, and Xu-Cun Ma, Phys. Rev. B **84**, 075335 (2011).
[22] Tanmay Das, Somnath Bhattacharyya, Bhanu Prakash Joshi, Arumugum Thamizhavel, and Srinivasan Ramakrishnan, Mater. Lett. **93**, 370 (2013).

[23] P. Larson and Walter R. L. Lambrecht, Phys. Rev. B **78**, 195207 (2008).
[24] Jian-Min Zhang, Wenguang Zhu, Ying Zhang, Di Xiao, and Yugui Yao, Phys. Rev. Lett. **109**, 266405 (2012).
[25] L. B. Abdalla, L. Seixas, T. M. Schmidt, R. H. Miwa, and A. Fazzio, Phys. Rev. B **88**, 045312 (2013).
[26] Jian-Min Zhang, Wenmei Ming, Zhigao Huang, Gui-Bin Liu, Xufeng Kou, Yabin Fan, Kang L. Wang, and Yugui Yao, Phys. Rev. B **88**, 235131 (2013).
[27] B. Ravel and M. Newville, J. Synchrotron Radiat. **12**, 537 (2005).
[28] G. Kresse and J. Hafner, Phys. Rev. B **48**, 13115 (1993); G. Kresse and J. Furthmüller, *ibid.* **54**, 11169 (1996); Comput. Mater. Sci. **6**, 15 (1996).
[29] G. Kresse and D. Joubert, Phys. Rev. B **59**, 1758 (1999).
[30] J. P. Perdew and Y. Wang, Phys. Rev. B **45**, 13244 (1992).
[31] W. Kohn and L. J. Sham, Phys. Rev. **140**, A1133 (1965).
[32] D. C. Koningsberger and R. Prins, *X-Ray Absorption: Principles, Applications, Techniques of EXAFS, SEXAFS and XANES* (John Wiley & Sons, Canada, USA, 1988), p. 40.
[33] R. W. G. Wyckoff, Cryst. Struct. **1**, 85 (1963); R. T. Downs and M. Hall-Wallace, The American Mineralogist Crystal Structure Database. American Mineralogist **88**, 247 (2003).
[34] M. Chevreton and F. Bertaut, C. R. Hebdomadaires Seances l'Acad. Sci. **253**, 145 (1961).
[35] S. Furuseth, A. Kjekshus, and A. F. Andresen, Acta Chem. Scand. **23**, 2325 (1969).
[36] F. J. Garcia-Garcia, A. K. Larsson, L. Noren, and R. L. Withers, Solid State Sci. **6**, 725 (2004).
[37] J. E. Hiller and W. Wegener, Neues Jahrbuch fur Mineralogie, Abhandlungen **94**, 1147 (1960).
[38] L. G. Berry, Am. Mineral. **39**, 504 (1954).
[39] V. Milman, Acta Crystallogr., Sect. B: Struct. Sci. **58**, 437 (2002).
[40] A. Kjekshus, T. Rakke, and A. Andresen, Acta Chem. Scand. A **28**, 996 (1974).
[41] R. D. Heyding and R. M. Murray, Can. J. Chem. **54**, 841 (1976).
[42] K. Sato, L. Bergqvist, J. Kudrnovsky, P. H. Dederichs, O. Eriksson, I. Turek, B. Sanyal, G. Bouzerar, H. Katavama-Yoshida, V. A. Dinh, T. Fukushima, H. Kizaki, and R. Zeller, Rev. Mod. Phys. **82**, 1633 (2010).